DOI: 10.13009/EUCASS2019-95

Structural design and analysis of a composite wing with high aspect ratio

Yu-shan Meng
College of Aerospace Science and Engineering, National University of Defense Technology, Changsha, Hunan 410073, China.
Li Yan
College of Aerospace Science and Engineering, National University of Defense Technology, Changsha, Hunan 410073, China. e-mail: scarlet@163.com
Wei Huang
College of Aerospace Science and Engineering, National University of Defense Technology, Changsha, Hunan 410073, China. e-mail: gladrain2001@163.com

Abstract
Due to the large bending moment and poor torsional stiffness of the wing with large aspect ratio, the large deformation cannot be avoided. The application of composite materials can improve the performance of the wing. Firstly, the design indexes of the wing with high aspect ratio are preliminarily formulated referring to some parameters of the Predator UAV and the finite element model is designed. Next, the aerodynamic analysis is performed and the static analysis is conducted in the ANSYS ACP module. Finally, two improvement schemes are proposed to deal with the problem that the wing with high aspect ratio would encounter.

1. Introduction

In the phylogeny of aeronautics, the wing plays an important role in the generation of lift force [1], and many scholars have paid attantion to its parametric design and optimization [2][3]. Once the stiffness of wing is insufficient during the flight, the wing will be over-deformed or even destroyed. At the same time, the unstable elastic effect is very dangerous [4], such as divergence, flutter and insufficient torsional rigidity, and they have always been prominent factors in reducing flight performance and stability, especially for wings with large aspect ratio. Eskandary et al. [5] investigated the aeroelastic properties of a cantilever wing with double bending and torsional vibrations and with large deflection ability in quasi-steady aerodynamics flows, and the influences of mass ratios and stiffness ratios were both taken into consideration. Duan and Zhang [6] developed a now approach to analyze the aeroelastic stability of a high-aspect-ratio wing based on the transfer function, and it is insentitive to mesh density and does not require structural modal analysis for aeroelastic stability. Farsadi et al. [7] studied the nonlinear aeroelastic behavior of pretwisted composite high aspect ratio wings, and it was structurally modeled as thin walled beams (TWB). Gunasekaran and Mukherjee [8] implemented a novel decambering technique to investigate the influence of wing twist on the induced drag of individual lifting surfaces by means of a vortex lattice approach. With the increase of the length of wings, the shear force and bending moment caused by the aerodynamic force will increase from the tip to the root. As a result, the tip of the wing will have a larger warpage deformation, and the wing will be fatigued and broken easily. A nonlinear method based on the computational fluid dynamic and computational structure dynamics (CFD/CSD) coupled approach was employed to analyze the nonlinear static aeroelastic and flutter characteristics of a composite wing with high aspect ratio, and the vertical and spanwise displacements and torsion angle of wing cross-sections are less than the linear result under the same fligh attitude [9].
The wing of UAV is a typical wing with large aspect ratio. Due to its long wingspan, the structural design problems of this wing are more significant. However, the strength of the wing cannot increase without limit, and excessive strength will lead to excessive conservative margin. This will not only increase the weight of the structure, but also decrease the performance of the aircraft. At the same time, this also explains the reason why the rigid is easy to bend. Only by combining rigidity with flexibility can we find the perfect midpoint between stiffness and structural performance. Therefore, a large number of composite materials are utilized in the wing with high aspect ratio in this paper. The application of composite materials with light weight and high strength can not only reduce the weight of the structure, but also make use of the elasticity of composite materials to realize the complex bending and torsion deformation of the wing, so as to meet the requirements of composite stiffness and strength of the structure [10]. The

DOI: 10.13009/EUCASS2019-95

application of composite materials enables the wing to produce greater compressive deformation like a shock absorber spring, and this increases the feasibility of bending or deformation of the wing.
Based on the information mentioned above, it is clear that the structural design and analysis of the composite wing with high aspect ratio has attracted an increasing attention, and it is very useful for the design of the aircraft. Therefore, in the current study, the composite wing with high aspect ratio has been designed and analyzed by means of the CFD/CSD coupled approach, and two approaches have been developed and employed to improve its performance, namely adding external device to the wing and adding winglets to the wing.

2. Aerodynamic analysis and structural design of the wing

Referring to some dimensions and flight parameters of the Predator UAV, the design parameters of the wing are preliminarily formulated as shown in Table.1.

Table.1 Design parameters of the wing employed in the current study.

Wingspan (m)	Root chord (m)	Tip chord (m)	Cruising Mach number	Aspect ratio	Flight height (m)
14.8	1.1	0.4	0.6	19.73	7620

The wing designed in this paper has a large span, and the flow around the tip of the airfoil will occur. The flow around the tip of the wing is a three-dimensional turbulent flow. Because there is no segmentation at the end of the wing, high-pressure airflow on the lower surface will bypass the tip and roll up to the upper surface. If the wingspan is longer, the flow around the tip is more obvious. In the current study, the NACA 2412 airfoil is chosen as the physical model.
The geometric model of the NACA 2412 airfoil drawn in CATIA is imported into ICEM CFD [11]. The generated meshes that meet the quality requirements are shown in Fig.1. For the post-processing of the calculation of the external flow field of the wing in this paper, the most notable thing is the lift and drag characteristics of the wing. Firstly, the aerodynamic analysis of NACA 2412 is carried out by the commercial software FLUENT. The flight parameters are imported, and the operating conditions are set. At the same time, the monitor is defined. After initializing the flow field, 3000 iteration steps are set up, and the CFD POST post-processing software is started to process the data after the iteration curve converges. The pressure contour of the airfoil is obtained as shown in Fig. 2.

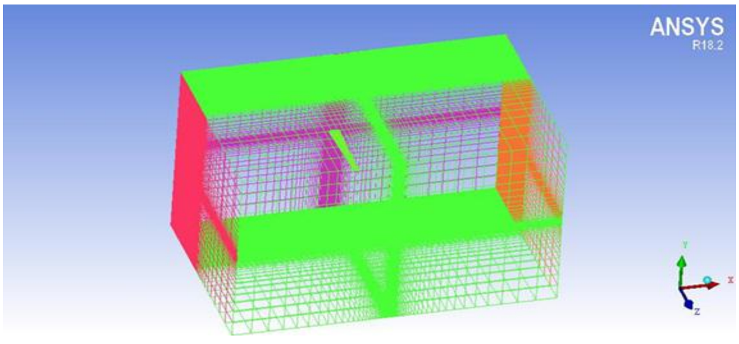

Figure 1. Structured mesh of NACA 2412.

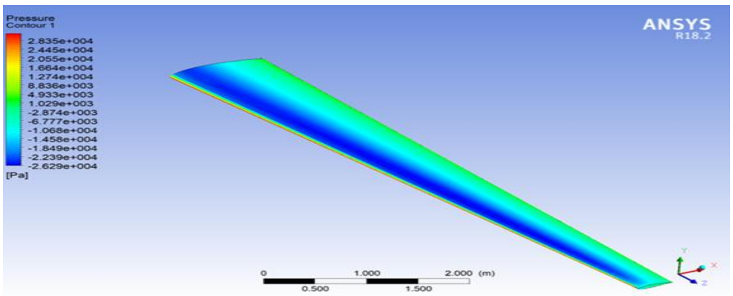

Figure 2. Pressure contour on the NACA 2412 airfoil.

DOI: 10.13009/EUCASS2019-95

The wing designed is simplified into a structure with only beams, ribs and skins. It adopts a double-beam structure with good bending and torsion rigidity to obtain a structural layout with high bearing efficiency [12]. As the main bearing member, the spar is essentially a shear beam, and the I-beam is used and arranged according to the equal percentage line. In practice, the skin of the wing can provide part of the flexural stiffness. Thus, the size of the beam will not be particularly large, and the desired results can be obtained by increasing the thickness of the skin. The widths of the upper and lower flanges of the fore-beam are both 110mm, and the thickness is 10mm. The rear beam acts as an auxiliary beam, and the widths of the upper and lower flanges are 80mm with its thickness being 10mm. The thickness of the web is 10mm as well. According to the characteristics of NACA 2412 airfoil and the bearing requirements of the structure, the front beam is placed 29% away from the leading edge and the rear beam 58% away from the leading edge.

In order to facilitate the analysis of the model, the ribs are simplified into a structure with only webs. It is known from engineering experience that the most suitable distance between the two nearest ribs is from 500mm to 600mm [13]. Here, the distance is chosen as 560mm. 14 wing ribs with the same structure are used, of which the root is a reinforced wing rib with a thickness of 9mm, and the others are common wing ribs with a thickness of 6mm. A weight reducing hole is arranged on the wing rib to reduce the weight of the structure. According to the size parameters proposed above, the model of the overall internal skeleton of the wing is established as shown in Fig. 3.

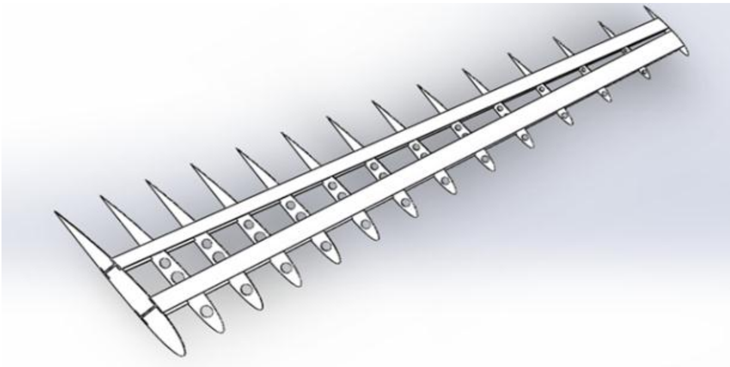

Figure 3. Model of the overall internal skeleton.

3. Finite element static analysis of the composite wing

In this paper, the finite element analysis of the wing is carried out in the Workbench collaborative simulation environment developed by ANSYS. The ANSYS Composite Pre/Post (ANSYS ACP) composite material special module is the pre and post-processing module of the composite material analysis scheme [14]. The ANSYS ACP module uses the micro-analysis approach to carry out the finite element modeling and material analysis. The structure can simulate the actual structure of the shell accurately, realize data transmission with other modules of ANSYS, and realize the design, manufacture and functional verification of composite products through the combination with the solver. The ACP module contains two sub-modules, namely pre-processing and post-processing. In the pre-processing module, all composite material definitions are created and mapped to the finite element grid. In the post-processing module, the resolving result file is imported into the process to evaluate and visualize the composite structure. The pre-and post-processing workflow is shown in Fig.4.

Figure 4. Pre- and post-processing workflow for finite element modeling and material analysis.

DOI: 10.13009/EUCASS2019-95

The simulation basis of the ACP Composite modeling module is the shell unit. The difference between the basic workflow of shell element and that of solid element is that when transferring data, the shell element needs to select the Transfer Shell Composite Data option to transfer the data of shell element to the static analysis module, which is actually the equivalent stiffness of multi-layer material. For composite shell element, the anisotropic laminated plate theory is used, and the finite element analysis is more complicated than the isotropic metal shell. When analyzing composite shell elements, we use the theory of anisotropic laminate thin shells, which is more complicated than the isotropic metal shell structure in the finite element analysis.

For the composite wing in this paper, the composite material structure is used for skin and wing rib, while the aluminum alloy material is used for beam structure to overcome the shortcomings of poor shear resistance of the composite material. The material parameters are shown in Tables.2 and 3.

Table 2 Properties of aluminum alloy.

ρ(Kg/m^3)	E(GPa)	μ	σ_b(Mpa)
2780	70610	0.3	432

Table 3 Properties of epoxy matrix composite.

ρ(Kg/m^3)	E_1(GPa)	E_2(GPa)	μ_{12}	G_{12}(GPa)
1600	181	10.3	0.28	7.17
X(MPa)	X'(MPa)	Y(MPa)	Y'(MPa)	S(MPa)
1500	700	40	246	68

According to the empirical formula, when the ratio of three ply angles (±45, 0, 90) is 60:30:10 for skin, the structure performance of the wing is the best. For the wing ribs, which are mainly subjected to the shear stress [15], ±45 is used entirely. The thickness and layer parameters of the ribs are formulated as follows.

Reinforced wing rib: the total thickness is 9mm; 6 layer groups; each group has 10 layers; the thickness of the single layer: t=0.15mm.

Normal wing rib: the total thickness is 6mm; 4 layer groups; each group has 10 layers; the thickness of the single layer: t=0.15mm.

After the stress analysis, the deformation cloud diagram and pressure cloud diagrams are obtained as Figs. 5-7.

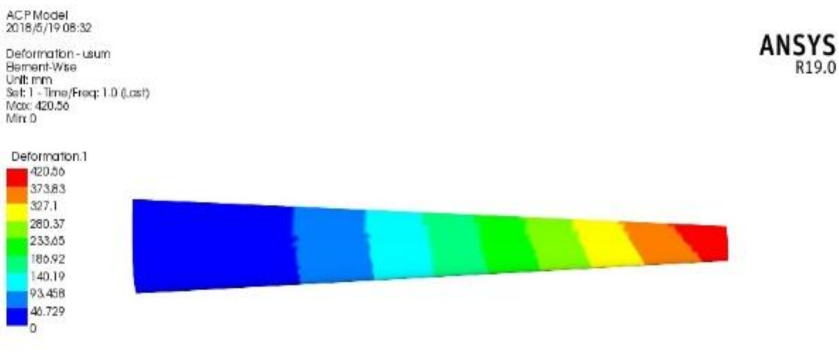

Figure 5. Deformation cloud diagram.

DOI: 10.13009/EUCASS2019-95

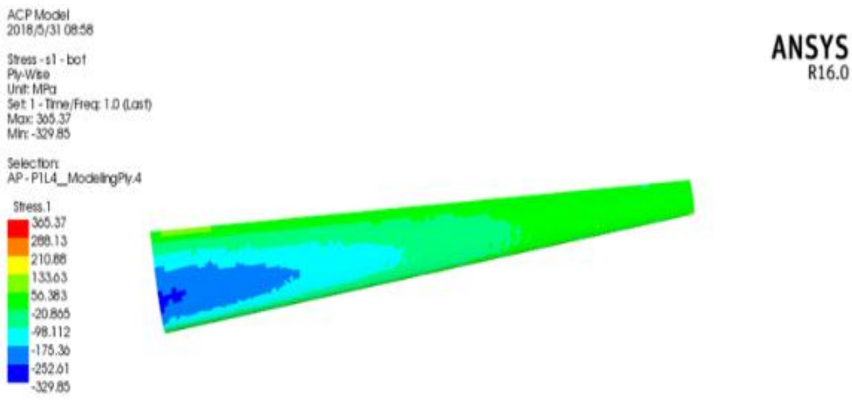

Figure 6. Pressure cloud diagram of the upper wing.

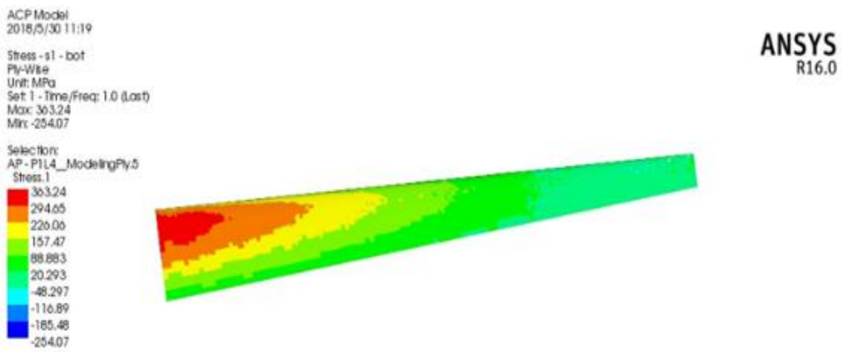

Figure 7. Pressure cloud diagram of the lower wing.

It can be obtained that the maximum deformation of the wing is 420.56mm, the maximum stress of the upper wing is 365.37Mpa, and the maximum layer stress of the lower wing is 363.24Mpa.

4. Optimization and improvement of the composite wing with high aspect ratio

In this paper, the deformation of the wing is relatively large. However, due to the current requirements of the composite material for the manufacturing process and the limitations of manufacturing costs, the application of composite wing structures has not been particularly extensive. Therefore, if the bending deformation of the wing need to be further reduced, some optimal improvement design can be conducted.

Two methods are used to improve the performance of the wing. The first method is to add external device to the wing in order to offset the upward momentum, and use the weight of the external device to offset a part of the lift of the wing so as to reduce the bending deformation trend of the wing. The second method is to add winglets to the wing tip in order to increase the effective span of the wing, thus improving the large bending deformation of the wing with high aspect ratio indirectly.

4.1 Add external device to the wing

The position of external device is usually determined by the pressure center of the wing, and it is usually placed at the front of the pressure center of the wing. After simulation in the commercial software FLUENT, the approximate position of the pressure center of the wing is 3.12m away from the root of the wing.

In the current study, the external device is regarded as a line load. Open the static analysis module, and load line pressure of 37.69N/mm uniformly on the line with the length of 380mm between the wing rib and the wing rib. The whole process is shown in Fig.8.

DOI: 10.13009/EUCASS2019-95

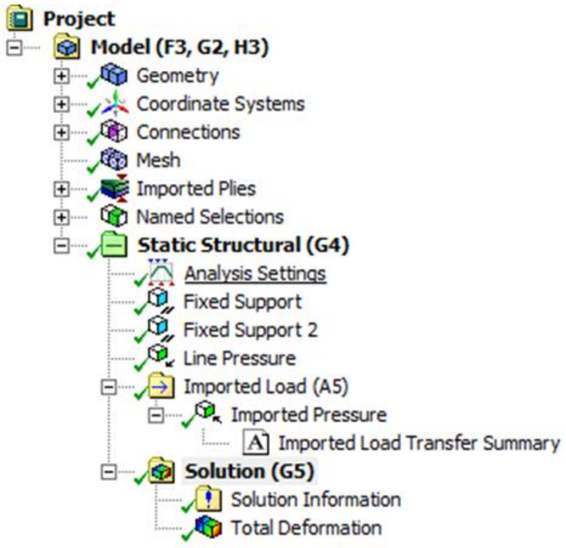

Figure 8. Whole process of the static analysis.

The location of the plug-in is varied separately. In order to show the location of the external service more intuitively, planar graphs as Cases 1-4 are shown in Fig.9.

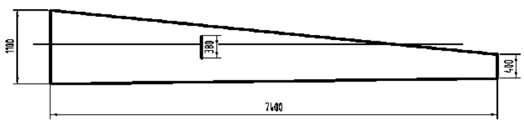

(a) Case 1

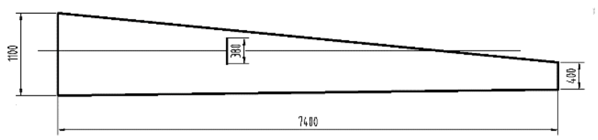

(b) Case 2

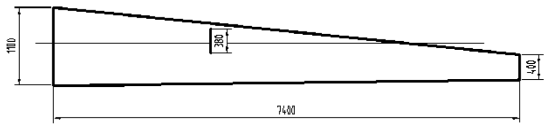

(c) Case 3

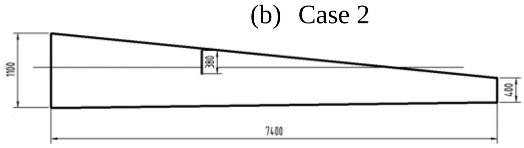

(d) Case 4

Figure 9. Planar graphs for different cases.

After applying the load, when the center of gravity of the external device is 20% behind the gravity line, the deformation cloud diagram and pressure cloud diagrams are obtained as Figs.10-12.

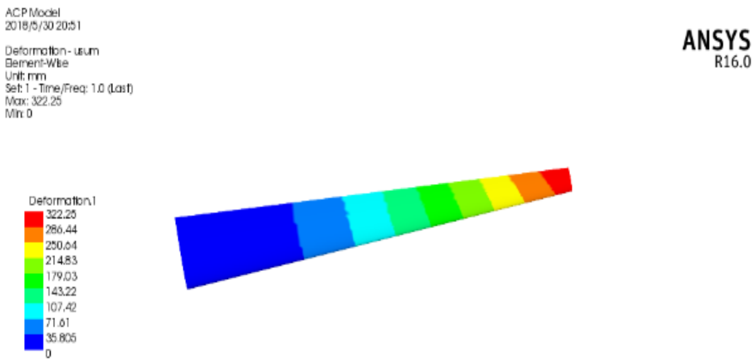

Figure 10. Deformation cloud diagram when the center of gravity of the external device is 20% behind the gravity line.

DOI: 10.13009/EUCASS2019-95

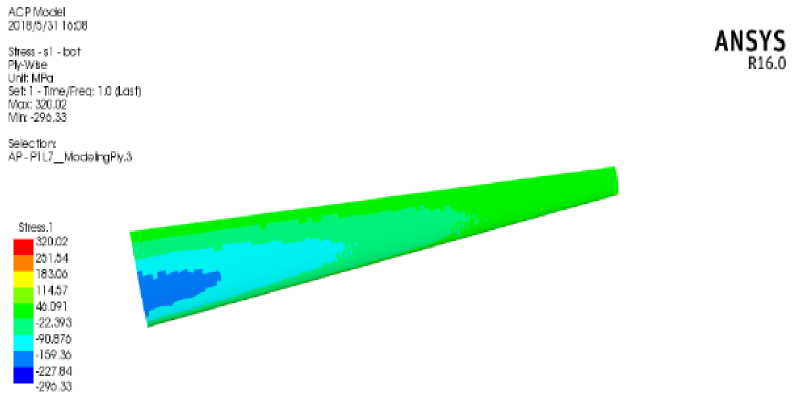

Figure 11. Pressure cloud diagram of the upper wing when the center of gravity of the external device is 20% behind the gravity line.

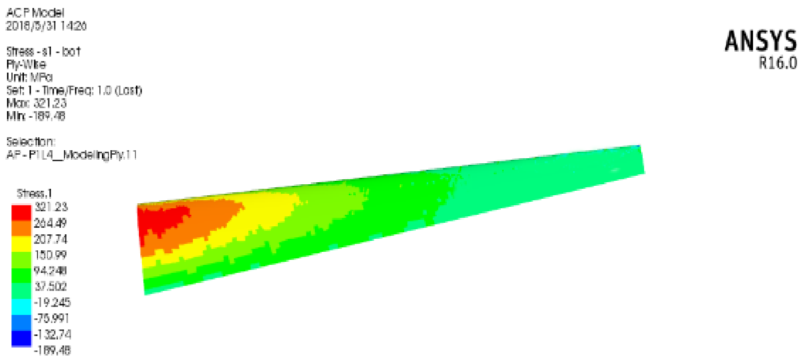

Figure 12. Pressure cloud diagram of the lower wing when the center of gravity of the external device is 20% behind the gravity line.

It can be obtained that the maximum deformation of the wing is 322.25mm, the maximum stress of the upper wing is 320.02Mpa, and the maximum layer stress of the lower wing is 321.23Mpa.

After applying the load, when the center of gravity of the external device is exactly on the gravity line, the deformation cloud diagram and pressure cloud diagrams are obtained as Figs.13-15.

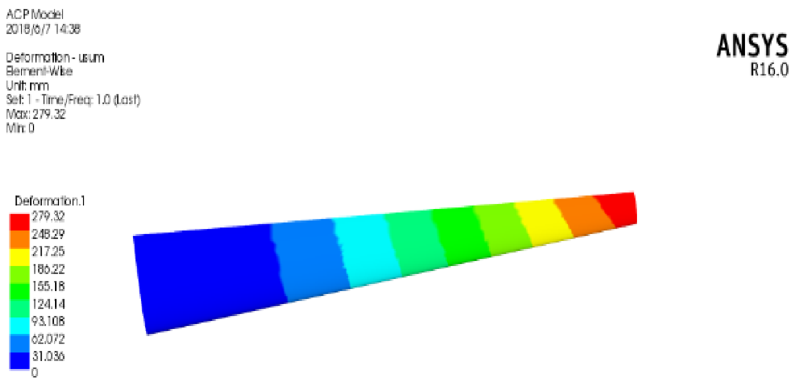

Figure 13. Deformation cloud diagram when the center of gravity of the external device is exactly on the gravity line.

DOI: 10.13009/EUCASS2019-95

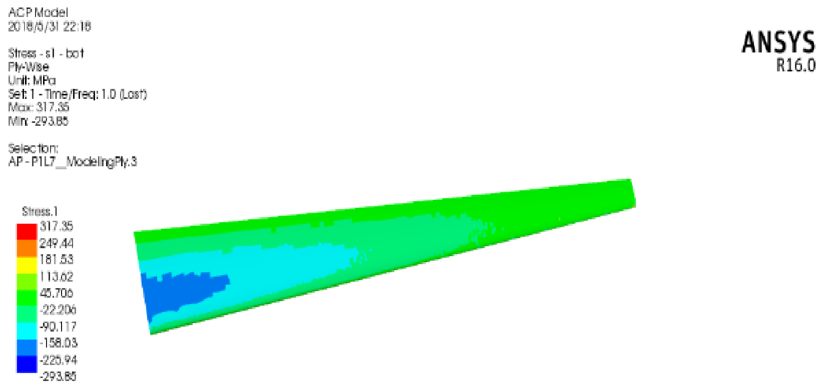

Figure 14. Pressure cloud diagram of the upper wing when the center of gravity of the external device is exactly on the gravity line.

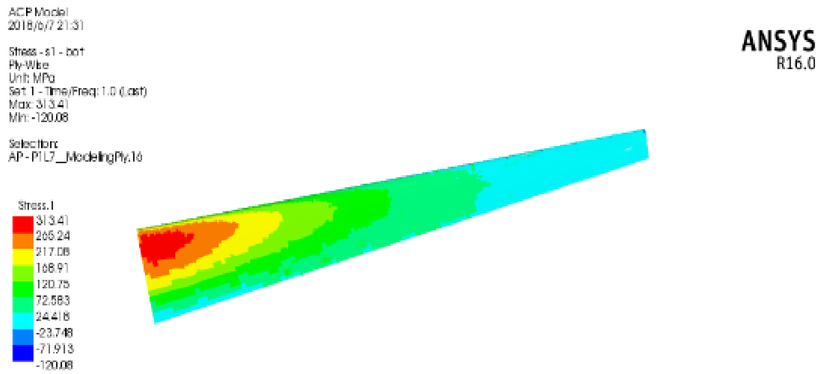

Figure 15. Pressure cloud diagram of the lower wing when the center of gravity of the external device is exactly on the gravity line.

It can be obtained that the maximum deformation of the wing is 279.32mm, the maximum stress of the upper wing is 317.35Mpa, and the maximum layer stress of the lower wing is 313.41Mpa.

After applying the load, when the center of gravity of the external device is 15% before the gravity line, the deformation cloud diagram and pressure cloud diagrams are obtained as Figs.16-18.

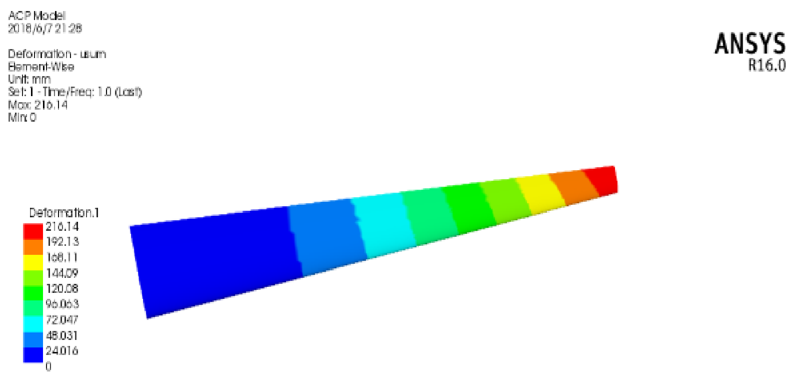

Figure 16. Deformation cloud diagram when the center of gravity of the external device is 15% before the gravity line.

DOI: 10.13009/EUCASS2019-95

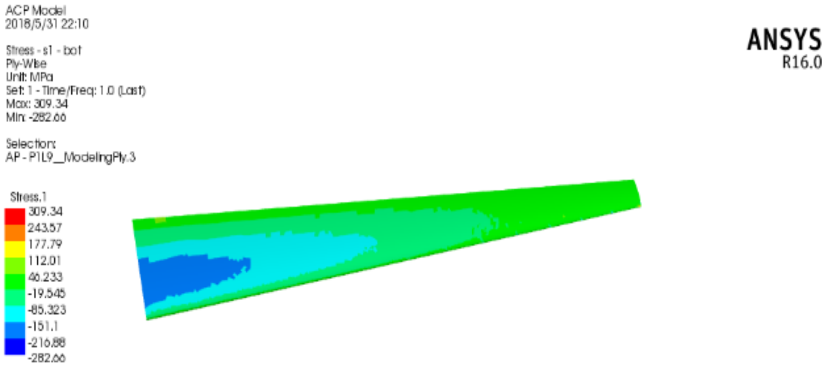

Figure 17. Pressure cloud diagram of the upper wing when the center of gravity of the external device is 15% before the gravity line.

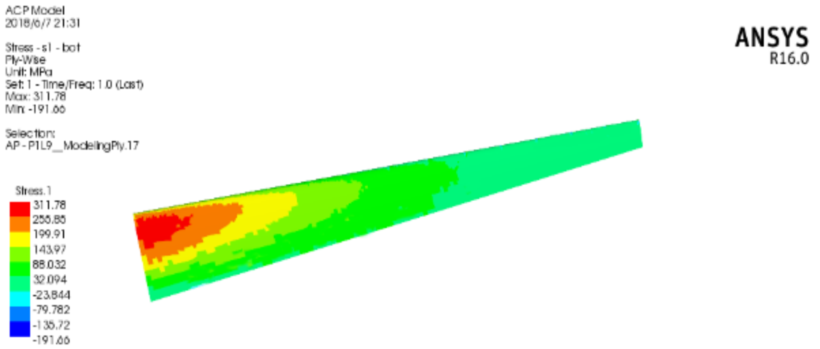

Figure 18. Pressure cloud diagram of the lower wing when the center of gravity of the external device is 15% before the gravity line.

It can be obtained that the maximum deformation of the wing is 216.14mm, the maximum stress of the upper wing is 309.34Mpa, and the maximum layer stress of the lower wing is 311.78Mpa.

After applying the load, when the center of gravity of the external device is 25% before the gravity line, the deformation cloud diagram and pressure cloud diagrams are obtained as Figs.19-21.

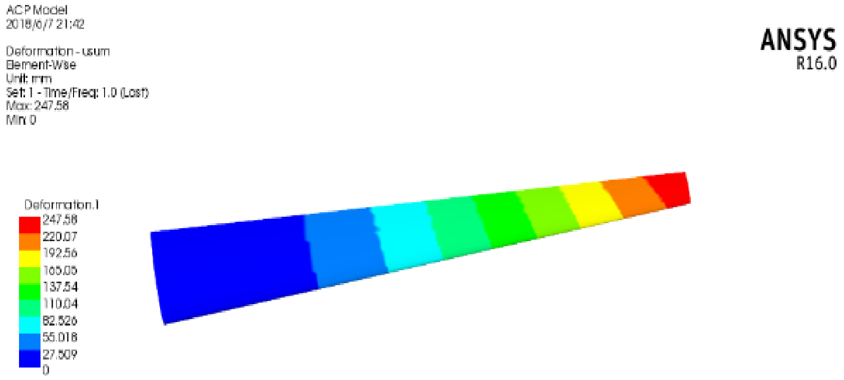

Figure 19. Deformation cloud diagram.

DOI: 10.13009/EUCASS2019-95

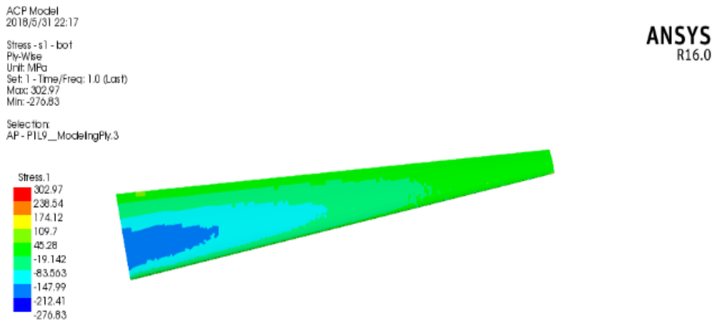

Figure 20. Pressure cloud diagram of the upper wing when the center of gravity of the external device is 25% before the gravity line.

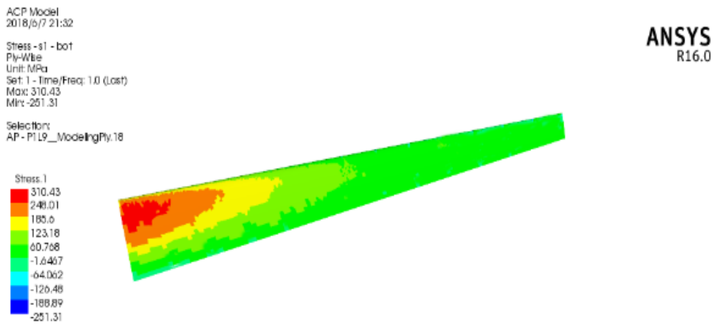

Figure 21. Pressure cloud diagram of the lower wing when the center of gravity of the external device is 25% before the gravity line.

It can be obtained that the maximum deformation of the wing is 247.58mm, the maximum stress of the upper wing is 302.97Mpa, and the maximum layer stress of the lower wing is 310.43Mpa.
When the center of gravity of the external device is at different positions of the gravity line, the results of deformation are summarized in Table.4 and polyline figure as Fig.22. In Table.4, the Unbalance rate is defined as the ratio of deformation difference of wings witn different materials to deformation of wings with metal materials.

Table 4. Deformation comparison for cases with external device at difference positions.

	20% behind the gravity line	on the gravity line	15% before the gravity line	25% before the gravity line
Maximum deformation (mm)	322.25	279.32	216.14	247.58
Initial deformation (mm)	420.56	420.56	420.56	420.56
Unbalance rate	23.38%	33.58%	48.61%	41.13%

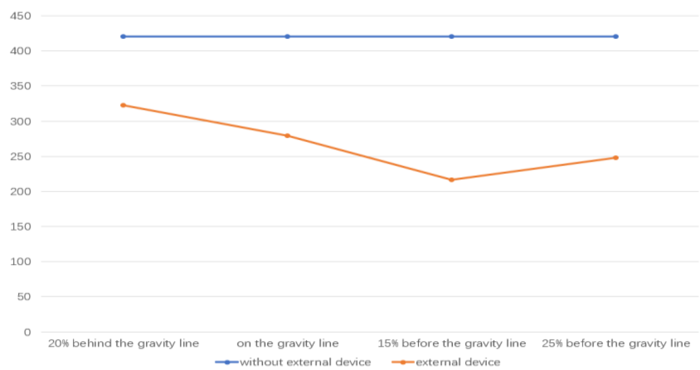

Figure 22. Maximum deformation for cases with external device at difference positions.

DOI: 10.13009/EUCASS2019-95

It can be seen from the difference ratio and the line chart in Table.1 and Fig.22 that the lift moment is partly offset by the weight of the external device itself. When the external device is at different positions, the maximum deformation of the wingtip decreases compared with the condition that there is no external device, and the maximum stresses of the upper and lower wing surfaces decrease. Especially, when the center of gravity of the external device is 15% before the gravity line, the deformation of the tip is the smallest, and the maximum deformation of the wing is 216.14 mm, which is 204.42 mm less than the initial deformation of the structure. When the center of gravity of the external stores is behind the center of gravity, the maximum deformation of the wing is 322.25mm, which is the smallest compared with the other positions. Therefore, when the load is applied and the wing is subjected to large deformation, the unfavorable deformation can be reduced by adding external device at 15% before the gravity line.

4.2 Add winglets to the wing

In addition to reducing the deformation of the wings by adding external device to the wings mentioned above, the performance of the wings can also be improved by changing the shape of the wing. As shown in Fig.23, the Boeing 787 adopts upward curved wings with carbon fiber structure to improve the performance of the aircraft.

Figure 23. Configuration of Boeing 787.

In this part, the winglet is adopted as the improvement device to improve the efficiency of the wing. This method not only increases the wingspan of the wing to a certain extent, but also reduces the airflow flowing from the lower surface of the wing to the upper surface and increases the lift-to-drag ratio. Fig.24 shows the shape of the wing after adding winglets with a height of 400mm.

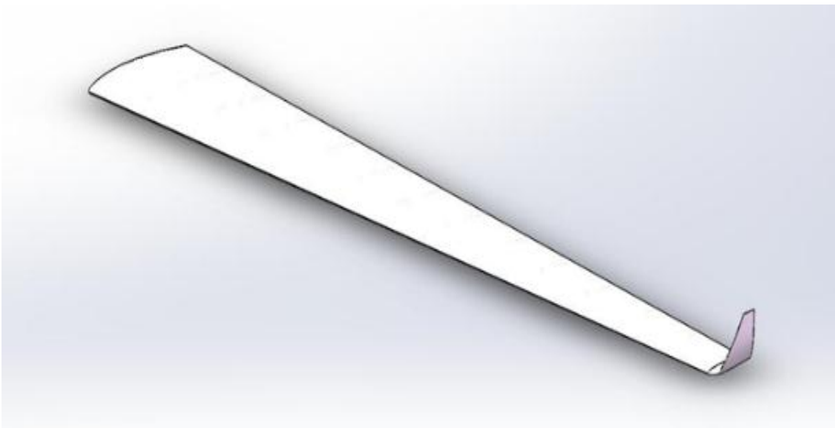

Figure 24. Shape of the wing with winglet.

Under the same load, the height of the winglet is varied to compare the performance of the wing. When the height of the winglet is 150mm, the deformation cloud diagram and pressure cloud diagrams are obtained as Figs. 25-27.

DOI: 10.13009/EUCASS2019-95

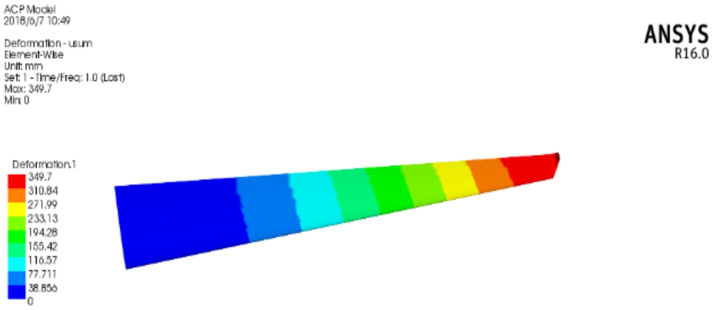

Figure 25. Deformation cloud diagram when the height of the winglet is 150mm.

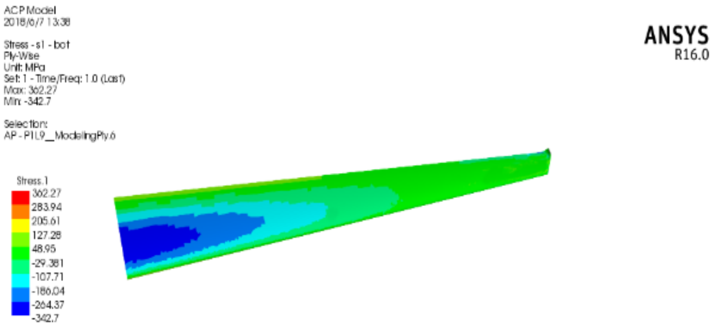

Figure 26. Pressure cloud diagram of the upper wing when the height of the winglet is 150mm.

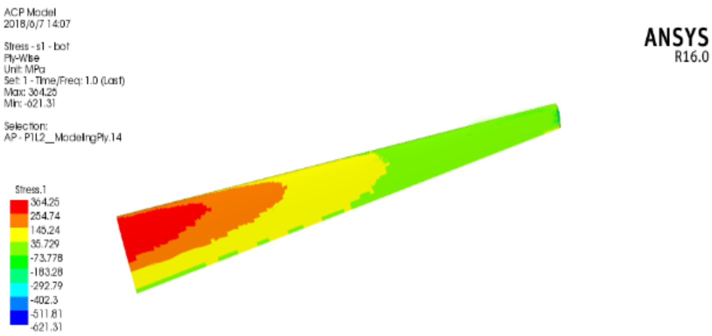

Figure 27. Pressure cloud diagram of the lower wing when the height of the winglet is 150mm.

In the following cases, the stresses on the upper and lower wing surfaces are of the same order, and they are all about 460 MPa. The maximum deformations with different heights of winglet are compared below.
When the height of the winglet changes from 200 mm to 400mm, the deformation cloud diagrams are obtained as Figs.28 (a)-(e).

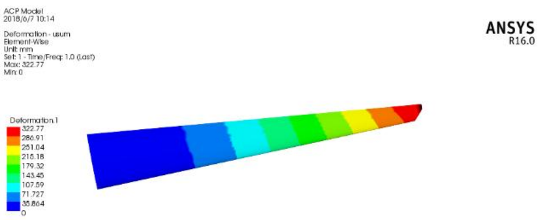

(a) 200mm

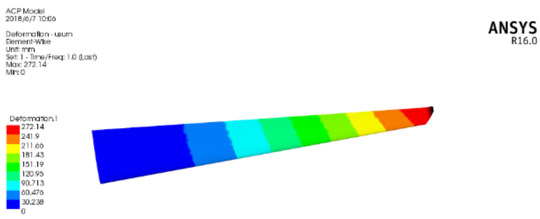

(b) 250mm

DOI: 10.13009/EUCASS2019-95

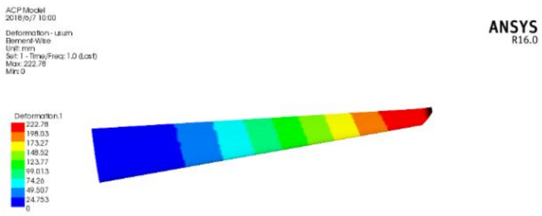

(c) 300mm

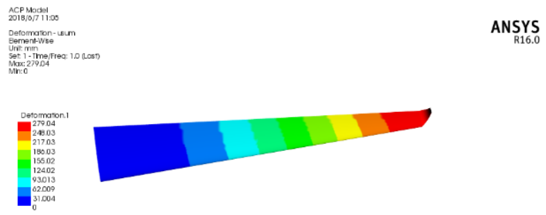

(d) 350mm

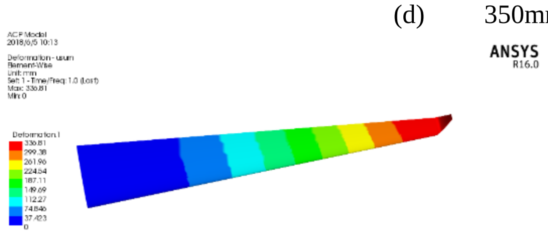

(e) 400mm

Figure 28. Deformation cloud diagrams for cases with different heights of winglet.

The analysis results of wings with different heights of winglet are listed as Table.5 and Fig.29.

Table 5. Deformation comparison for cases with different heights of winglet.

	Maximum deformation (mm)	Initial deformation (mm)	Unbalance rate
150mm	349.7	420.56	16.85%
200mm	322.22	420.56	23.25%
250mm	272.77	420.56	35.14%
300mm	222.78	420.56	47.02%
350mm	279.04	420.56	33.65%
400mm	336.81	420.56	19.91%

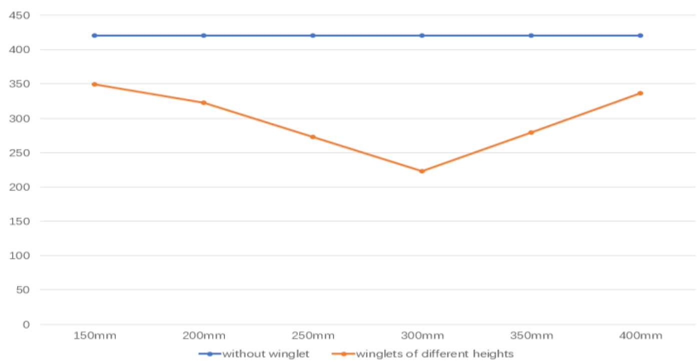

Figure 29. Maximum deformation for cases with different heights of winglet.

From the data in Table.2 and the trend of the line chart in Fig.29, it can be seen that the maximum deformation of the tip of the wing decreases when the winglet is added to the wingtip, but the height of the winglet is not the higher the better. When the height of the winglet is 300 mm, the maximum deformation of the wing decreases the most, and this is 197.78mm less than the original one. Therefore, it is concluded that for the composite wing designed in this paper, the maximum deformation of the wing can be reduced by adding the winglet with its height being 300 mm to the wing.

DOI: 10.13009/EUCASS2019-95

5. Conclusions

This paper aims to design a composite wing with large aspect ratio. Firstly, the aerodynamic shape of the wing is designed, and the structure type and component dimensions are proposed initially. The structural finite element static analysis is carried out in the ACP module of ANSYS Workbench by using the aerodynamic load obtained. In view of the inevitable structural deformation problem of the wing in process of flight, considering the cost limitation and feasibility of manufacturing process, two improvement schemes are proposed at the end of this paper.

The first design scheme is to add external device to the wing in order to offset the upward momentum, and use the weight of the external device to offset a part of the lift of the wing so as to reduce the bending deformation trend of the wing. Especially, when the center of gravity of the external device is 15% before the gravity line, the deformation of the tip is the smallest, and this is 204.42 mm less than the initial deformation of the structure.

The second design scheme is to add winglet at the tip of the wing to increase the effective span of the wing, thus improving the large bending deformation of the wing with high aspect ratio indirectly in this paper. When the height of the winglet is 300 mm, the maximum deformation of the wing decreases the most.

Conflict of interest statement

The authors declare there is no conflict of interest regarding the publication of this paper.

Acknowledgments

The authors would like to express their thanks for the support from the National Natural Science Foundation of China (No.11502291).

References

[1]. Sziroczak D, Smith H. A review of design issues specific to hypersonic flight vehicles. Progress in Aerospace Sciences, 2016, 84: 1-28

[2]. Zhang T T, Wang Z G, Huang W, Yan L. A review of parametric approaches specific to aerodynamic design process. Acta Astronautica, 2018, 145: 319-331

[3]. Zhang T T, Huang W, Wang Z G, Yan L. A study of airfoil parameterization, modeling, and optimization based on the computtional fluid dynamics method. Journal of Zhejiang University – Science A (Applied Physics & Engineering), 2016, 17(8): 632-645

[4]. Cesnik C E S, Hodges D H, and Patil M J. Nonlinear aeroelastic analysis of aircraft with high-aspect-ratio wings. New York: AIAA, 1998, AIAA-98-1995

[5]. Eskandary K, Dardel M, Pashaei M H, Moosavi A K. Nonlinear aeroelastic analysis of high-aspect-ratio wings in low subsonic flow. Acta Astronautica, 2012, 70: 6-22

[6]. Duan J B, Zhang Z Y. Aeroelastic stability analysis of aircraft wings with high aspect ratios by transfer function method. International Journal of Structural Stability and Dynamics, 2018, 18(12): 1850150

[7]. Farsadi T, Rahmanian M, Kayran A. Geometrically nonlinear aeroelastic behavior of pretwisted composite wings modeled as thin walled beams. Journal of Fluids and Structures, 2018, 83: 259-292

[8]. Gunasekaran M, Mukherjee R. Behaviour of trailing wing(s) in echelon formation due to wing twist and aspect ratio. Aerospace Science and Technology, 2017, 63: 294-303

[9]. Qiao S J, Gao H S, Lyu Y, Hua L, Wang F S. Nonlinear aeroelatic characteristics analysis of composite wing with high aspect ratio based on co-rorational method. Journal of Fluids and Structures, 2018, 82: 619-637

[10]. Institute of Science and Technology, ministry of aerospace industry. Composite material structure design manual. Beijing: Aviation industry press, 1990.

[11]. Ji B B, Chen J P. ANSYS ICEM CFD grid generation technology. Beijing: China WaterPower Press, 2012: 20-22.

[12]. Zhang J K, Li Z N, Kou C H, Design and research of high aspect ratio composite wing structure. Journal of Aeronautics, 2005, 26(4): 450-453.

[13]. Zhao A Y. The layout of ribs in the wingbox for modern civil aircraft. Science & Technology Vision, 2012.

[14]. Zhan Y L. Finite element analysis and application of composite materials based on ANSYS. Beijing: China WaterPower Press, 2017: 32-34.

[15]. The Editorial board of Aircraft design manual. Aircraft Design Manual (the tenth volume). Beijing: Aviation Industry Press, 2000.